room temperature. The dark brown residue was dissolved in 1:1 THF/CH_2Cl_2 (40 mL), filtered to remove ruthenium metal, evaporated, columned through SiO_2 (eluting with 1% THF/CH_2Cl_2), and evaporated to yield copper red crystals (62 mg, 93%). NMR (CD_2Cl_2) 9.97 (2 H, s), 9.94 (2 H, s), 4.34 (4 H, t), 4.04 (4 H, q), 3.64 (6 H, s), 3.60 (6 H, s), 3.59 (6 H, s), 3.28 (4 H, t), 1.89 (6 H, t), 1.03 (4 H, br s), 0.11 (4 H, br s); UV-vis 390, 516, 548 nm; IR ν_{CO} (CH_2Cl_2) 1928 cm^{-1}; m/z isotopic distributions centered on 722.4 (M^+) and 694.4 ($M - CO^+$); $C_{37}H_{40}O_5N_4Ru$ requires M^+ = 721.9 and $C_{36}H_{40}O_4N_4Ru$ requires M^+ = 693.9.

Analysis of Titration Data. In the titrations it is not possible to measure independently the absorption of the 1:1 and 2:1 complexes for the monofunctional ligands binding to the dimers. This can lead to interpretation errors when dealing with sequential binding at a single site,[21] but we have two separate sites whose properties are identical. As a starting point we assumed that to a good approximation, the extinction coefficients of the 1:1 complexes at any wavelength are given by

$$\epsilon(1{:}1\ \text{complex}) = 0.5\ \epsilon(\text{free dimer}) + 0.5\ \epsilon(2{:}1\ \text{complex}) \quad (12)$$

The absorption of the dimer is in effect the sum of the absorptions of the two porphyrin units. Justification for this assumption comes from curve-fitting routines: using the above values for the 1:1 complex extinction coefficients yields a much better fit to the data than any other values. For bifunctional ligands we assumed

$$\epsilon(1{:}1\ \text{complex bound inside cavity}) = \epsilon(2{:}1\ \text{complex}) \quad (13)$$

This is reasonable where the degree of exciton coupling is negligible. With DABCO, **4**, the 1:1 complex is observable directly, and no assumptions are required; with 4,4'-dipyridyl **17** an additional factor of 0.85 gave the best fit (see Results). The following equation and the titration data were used to determine if there was cooperativity in binding to the dimers:

$$\ln\{(A - A_0)/(A_f - A)\} = x \ln [\text{free ligand}] + \ln K \quad (14)$$

where A is the absorption at a particular wavelength, λ; A_0 is the initial absorption at λ; A_f is the final absorption at λ; K is the binding constant; and x is a constant which defines the number of ligands bound per site. A plot of $\ln\{(A - A_0)/(A_f - A)\}$ vs ln [free ligand] yields a straight line of slope 1 for independent, identical binding at the two sites. Cooperative binding, where the second binding is aided by the first, gives $x > 1$, while negative cooperativity gives $x < 1$.

The data were also analyzed by using a least-squares curve-fitting routine. For systems exhibiting cooperativity this was essential in order to obtain accurate binding constants; in simpler systems, these curve-fitting results merely confirmed those obtained by the above analysis. The data were analyzed by using the expression

$$A = \frac{A_0 + K_1[L]A_1 + K_1K_2[L]^2A_2}{1 + K_1[L] + K_1K_2[L]} \quad (15)$$

where A_0 = absorbance for free dimer at λ; A_1 = absorbance for 1:1 complex at λ; A_2 = absorbance for 2:1 complex at λ. The other symbols have the same meaning as above. The expression

$$A = \frac{A_0 + K_1^{\text{out}}[L]\{0.5A_0 + 0.5A_2\} + K_1^{\text{in}}[L]0.85A_2 + 0.5(K_1^{\text{out}})^2[L]^2A_2}{1 + K_1^{\text{out}}[L] + K_1^{\text{in}}[L] + 0.5(K_1^{\text{out}})^2[L]^2} \quad (16)$$

was used to fit the data from the titrations of **17** to take into account the equilibrium between binding on the outside and on the inside of the dimers in the 1:1 complexes. This equation (less the correction factor of 0.85) also fitted the data for the other ligands and confirmed that, over most of the titration, all except pyrazine were bound exclusively inside the cavity.

Acknowledgment. We thank the SERC (UK) and Department of Education (Northern Ireland) for financial support and Dr. A. Crawford for the Simplex routines.

Electron Paramagnetic Resonance and Electrochemical Study of the Oxidation Chemistry of Mononuclear and Binuclear Chromium Carbonyl Thiolates†

Jerry Springs,‡ Christopher P. Janzen,‡ Marcetta Y. Darensbourg,*,‡ Joseph C. Calabrese,§ Paul J. Krusic,*,§ Jean-Noël Verpeaux,∥ and Christian Amatore*,∥

Contribution from the Department of Chemistry, Texas A&M University, College Station, Texas 77843, the Central Research and Development Department, E. I. du Pont de Nemours and Company, Experimental Station, Wilmington, Delaware 19880-0328, and the Laboratoire de Chimie (CNRS-UA 1110), Ecole Normale Supérieure, 75231 Paris Cedex 05, France.
Received November 27, 1989

Abstract: The oxidation chemistry of $RSCr(CO)_5^-$ thiolate anions, $1(R)^-$, and of their binuclear analogues $RS[Cr(CO)_5]_2^-$, $2(R)^-$, has been studied by cyclic voltammetry, EPR, and low-temperature IR. Rapid potential scan cyclic voltammetry shows that the radicals $1(R)^\bullet$ have lifetimes of less than 50 μs and decay by first-order kinetics. Chemical studies are consistent with fragmentation of $1(R)^\bullet$ into an alkylthiyl radical $RS^\bullet$ and a $Cr(CO)_5$ fragment. The slower reactions following the initial irreversible oxidation have been elucidated by cyclic voltammetry. The major product of chemical and electrochemical oxidation of $1(R)^-$ is the monodentate disulfide complex $(RS-SR)Cr(CO)_5$ formed by complexation of $Cr(CO)_5$ fragments to the organic disulfide resulting from dimerization of $RS^\bullet$ radicals. The electrochemical oxidation of $2(R)^-$ proceeds in two chemically reversible steps to the corresponding $2(R)^\bullet$ radicals and $2(R)^+$ sulfonium cations. The intensely colored $2(R)^\bullet$ radicals have limited thermal stability and were characterized by EPR, low-temperature IR, and extended Hückel MO calculations. The unpaired electron resides to a large extent in a p-type orbital on the trigonal sulfur, which is π-conjugated to d orbitals of the neighboring Cr atoms. This orbital is part of a three-center pseudoallylic π system occupied by five electrons, totally analogous to that with four-electron occupancy put forward previously for binuclear phosphinidene complexes $RP[ML_n]_2$, e.g., $RP[Cr(CO)_5]_2$, which is isoelectronic with $2(R)^+$. The X-ray structures of t-$BuSCr(CO)_5^-$ and t-$BuS[Cr(CO)_5]_2^-$ are also presented.

Introduction

Although most well-known chemical reactions of transition-metal complexes involve transformations occurring at the metal center, ligand-centered reactions can offer important alternative features of reactivity. Transition-metal thiolato complexes, supported by carbonyl ligands, offer an opportunity to examine ligand- vs metal-based reactivity, both by experiment and theory. For example, the Fe(II) complexes $(\eta^5\text{-}C_5H_5)Fe(CO)_2(SAr)$ (Ar = C_6H_5 and $p\text{-}C_6H_4X$) have been shown to be chemically active toward nucleophiles via sulfur lone-pair reactivity in accord with

† Du Pont contribution no. 5354.
‡ Texas A&M University.
§ E. I. du Pont de Nemours and Co.
∥ Ecole Normale Supérieure.

0002-7863/90/1512-5789$02.50/0

Scheme I

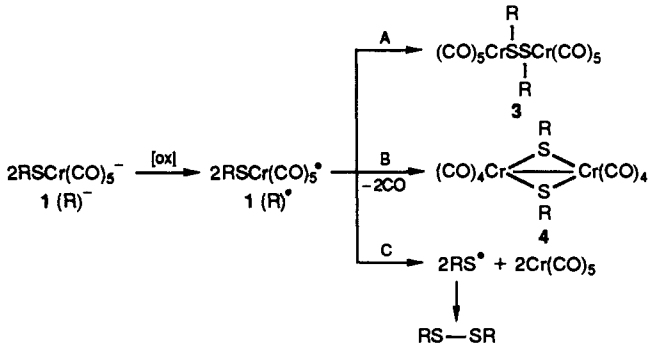

Fenske–Hall molecular orbital calculations, which show the HOMO to have mainly sulfur 3p character.[1] Theory also suggests that the odd electron of the related radical cations $(\eta^5\text{-}C_5H_5)Fe(CO)_2(SR)^{\bullet+}$ is largely localized on sulfur. Accordingly, one-electron oxidation of $(\eta^5\text{-}C_5H_5)Fe(CO)_2(SR)$ has been shown to result in coupling of the metal-bound SR groups, yielding $[(\eta^5\text{-}C_5H_5)Fe(CO)_2(\mu\text{-}RSSR)Fe(CO)_2(\eta^5\text{-}C_5H_5)]^{2+}$.[2] This coupling becomes reversible, if a CO is replaced by phosphine ligands,[2,3] or may not occur at all, allowing the isolation and spectroscopic characterization of the monomeric radical cation, if both CO ligands of $(\eta^5\text{-}C_5H_5)Fe(CO)_2(SR)$ are replaced with phosphine ligands.[4] The isoelectronic neutral radical $[\eta^5\text{-}C_5(CH_3)_5]Mn(CO)_2(SR)^{\bullet}$ (R = *t*-Bu) can also be isolated in monomeric form.[5] Presumably, the steric protection provided by the pentamethylcyclopentadienyl group and the *t*-Bu group now impedes coupling at the sulfur radical centers.

For this series of thiolate complexes, no evidence was reported for oxidative coupling at the metal centers which could lead, after loss of CO, to the well-known dimers with two bridging RS groups exemplified by $[(\eta^5\text{-}C_5H_5)Fe(CO)SR]_2$.[6] Such oxidative coupling of metal centers accompanied by CO loss has indeed been observed very recently in the oxidation of the trigonal-bipyramidal thiolate anion $PhSFe(CO)_4^-$.[7] This oxidation yielded the metal–metal bonded dimer $(CO)_3Fe(\mu\text{-}SPh)_2Fe(CO)_3$ and no products resulting from coupling at the sulfur atoms, even though the singly occupied molecular orbital (SOMO) in the presumed radical intermediate $PhSFe(CO)_4^{\bullet}$ should also have substantial sulfur 3p character.[8]

Surprisingly, almost nothing is known about the oxidative chemistry of group VI metal carbonyl thiolates $RSM(CO)_5^-$ (M = Cr, Mo, and W) which, together with their binuclear analogues $RS[M(CO)_5]_2^-$, have been known for over 20 years.[9,10] Noteworthy in this connection, however, is a report of a thermally labile paramagnetic material to which the structure $HSCr(CO)_5^{\bullet}$ was assigned.[9] In view of the bonding equivalence of three CO's with $(\eta^5\text{-}C_5H_5)^-$, such a radical would be the electronic equivalent of the hypothetical radical anion $(\eta^5\text{-}C_5H_5)Cr(CO)_2SR^{\bullet-}$, which is in turn isoelectronic with $(\eta^5\text{-}C_5H_5)Mn(CO)_2SR^{\bullet}$ and $(\eta^5\text{-}C_5H_5)Fe(CO)_2SR^{\bullet+}$, whose propensity to couple at the sulfur atom was pointed out above. Intrigued by this report and wishing to extend our understanding of the oxidative chemistry of metal carbonyl thiolates, particularly as regards ligand- vs metal-center

Scheme II

$$RS[Cr(CO)_5]_2^- \underset{+e}{\overset{-e}{\rightleftharpoons}} RS[Cr(CO)_5]_2^{\bullet} \underset{+e}{\overset{-e}{\rightleftharpoons}} RS[Cr(CO)_5]_2^+$$
$$2\,(R)^- \qquad 2\,(R)^{\bullet} \qquad 2\,(R)^+$$

reactivity, we decided to examine in some detail the chemical and electrochemical oxidation of a series of mononuclear and binuclear chromium carbonyl thiolates, $RSCr(CO)_5^-$ (**1**$(R)^-$) and $RS[Cr(CO)_5]_2^-$ (**2**$(R)^-$), and to characterize, if possible, the radical intermediates by electron paramagnetic resonance (EPR). For the mononuclear thiolates we anticipated three possibilities following one-electron oxidation (Scheme I): (A) formation of sulfur–sulfur coupled dimers **3**, (B) metal–metal coupling with CO loss leading to thiolato-bridged dimers **4**,[11] and (C) homolysis of the Cr–S bond to yield a short-lived alkylthiyl radical and a coordinatively unsaturated $Cr(CO)_5$ fragment; the alkylthiyl radicals would then dimerize by essentially diffusion-controlled kinetics to yield the corresponding organic disulfide.[12]

In this report we present evidence indicating that the chemical and electrochemical oxidation of **1**$(R)^-$ follows only path C. The intermediate radicals **1**$(R)^{\bullet}$ have lifetimes of less than 50 μs and could not be detected by EPR. The oxidation of the binuclear analogues $RS[Cr(CO)_5]_2^-$, on the other hand, proceeds reversibly in two steps (Scheme II) and gives rise to deeply colored novel radicals **2**$(R)^{\bullet}$ of limited thermal stability, which were characterized by EPR and by extended Hückel MO calculations, and novel organometallic sulfonium cations **2**$(R)^+$, isoelectronic with the well-known binuclear phosphinidene complexes[13] of which $RP[Cr(CO)_5]_2$ (R = *tert*-butyl, mesityl)[14,15] are representative examples.

Experimental Section

1. Methods and Materials. All preparations and reactions were carried out with rigorous exclusion of air and moisture, utilizing Schlenk and glovebox techniques. Nitrogen was purified over an on-line column consisting of molecular sieves, calcium chloride, and calcium sulfate. Tetrahydrofuran (THF) and hexane were distilled from sodium/benzophenone ketyl. Methylene chloride was refluxed over calcium hydride. Diethyl ether was dried and distilled from $LiAlH_4$. All solvents were used immediately following distillation or were stored under nitrogen over molecular sieves. The ^{13}CO gas (98% enrichment) was purchased from Mound Laboratories. All other reagents were purchased from standard vendors as reagent or better grades and used without further purification.

Infrared spectra were measured by using 0.10-mm CaF_2 solution cells on an IBM FTIR 32 or a Perkin-Elmer 983 G spectrometer. ESR spectra were recorded with a Bruker ER420 spectrometer equipped with accessories to measure precisely the microwave frequency and the magnetic field. An unsilvered Dewar system of conventional design was used to vary the temperature of the samples.

Low-temperature infrared spectra were obtained by using a standard 0.10-mm NaCl solution cell with circular aperture (Wilmad 116-3) and 0.1-mm Teflon spacers mounted flush against a 10-mm brass block as a heat sink to slow the warming of solutions in the cell. The brass block has a slot in its center to allow the IR beam to pass through the NaCl window and was fitted with a thermocouple inserted into a small hole in the block. Typically, the cell assembly was cooled to the desired low temperature in a refrigerated well of a modified Vacuum Atmospheres glovebox together with the solutions to be reacted at low temperatures. After being mixed, the solutions were transferred with a chilled syringe

(1) Ashby, M. T.; Enemark, J. H.; Lichtenberger, D. L. *Inorg. Chem.* **1988**, *27*, 191.
(2) (a) Treichel, P. M.; Rosenhein, L. D. *J. Am. Chem. Soc.* **1981**, *103*, 691. (b) Treichel, P. M.; Rosenhein, L. D.; Schmidt, J. S. *Inorg. Chem.* **1983**, *22*, 3960.
(3) Treichel, P. M.; Rosenhein, L. D. *Inorg. Chem.* **1984**, *23*, 4018.
(4) Treichel, P. M.; Molzahn, D. C.; Wagner, K. P. *J. Organomet. Chem.* **1979**, *174*, 191.
(5) Winter, A.; Huttner, G.; Zsolnai, L.; Kroneck, P.; Gottlieb, M. *Angew. Chem., Int. Ed. Engl.* **1984**, *23*, 975.
(6) For a review of FeS complexes, see: Markó, L.; Markó-Monostory, B. In *The Organic Chemistry of Iron*; Academic Press: New York, 1981; Vol. 2, p 283.
(7) Liaw, W.-F.; Kim, C.; Darensbourg, M. Y.; Rheingold, A. L. *J. Am. Chem. Soc.* **1989**, *111*, 3591.
(8) Riordan, C. G.; Darensbourg, M. Y., unpublished results.
(9) (a) Behrens, H.; Lindner, E.; Birkle, S. *Z. Anorg. Allg. Chem.* **1969**, *369*, 132. (b) Behrens, H. *Adv. Organomet. Chem.* **1980**, *18*, 1.
(10) Ruff, J. K.; King, R. B. *Inorg. Chem.* **1969**, *8*, 180.
(11) Several examples of such dimers and their dianions are known for W and Mo: (a) Hohmann, M.; Krauth-Siegel, L.; Weidenhammer, K.; Schultze, W.; Ziegler, M. L. *Z. Anorg. Allg. Chem.* **1981**, *481*, 95. (b) Winter, A.; Scheidsteger, O.; Huttner, G. *Z. Naturforsch.* **1983**, *38B*, 1525. (c) Zhuang, B.; McDonald, J. W.; Schultz, F. A.; Newton, W. E. *Organometallics* **1984**, *3*, 943. (d) Darensbourg, D. J.; Sanchez, K. M.; Reibenspies, J. *Inorg. Chem.* **1988**, *27*, 3636.
(12) (a) For a recent kinetic study of alkylthiyl radicals, see: McPhee, D. J.; Campredon, M.; Lesage, M.; Griller, D. *J. Am. Chem. Soc.* **1989**, *111*, 7563. (b) For a general review of organic sulfur radicals, see: Lunazzi, L.; Pedulli, G. F. In *Organic Sulfur Chemistry*; Bernardi, F., Csizmandia, I. G., Mangini, A., Ed.; Elsevier: New York, 1985; p 484.
(13) For a review, see: Huttner, G.; Evertz, K. *Acc. Chem. Res.* **1986**, *19*, 406.
(14) Huttner, G.; Borm, J.; Zsolnai, L. *J. Organomet. Chem.* **1984**, *263*, C33.
(15) Lang, H.; Orama, O.; Huttner, G. *J. Organomet. Chem.* **1985**, *291*, 293.

into the cold IR cell. To avoid moisture condensation, the cell was placed under N_2 in a glass jar on an insulating pad and was rapidly transferred to the N_2-flushed sample compartment of the IR spectrometer. The nitrogen flush of the IR sample compartment was increased to minimize the condensation of moisture on the cell.

The low-temperature photoreactor consisted of a standard quartz Dewar for variable-temperature ESR surrounded by the coils of a low-pressure Hg discharge tube (mostly 254-nm UV) in the shape of a tight spiral. The cooling was provided by a flow of cold nitrogen.

2. Preparations. A. [PPN][RSCr(CO)$_5$] ([PPN][1(R)]); R = *t*-C$_4$H$_9$, C$_2$H$_5$, *i*-C$_3$H$_7$. In a typical synthesis, 1.5 g (1.96 mmol) of [PPN][Cr(CO)$_5$Cl] was added to a N_2-filled 100-mL Schlenk flask along with 0.22 g (1.96 mmol) of [Na][*t*-C$_4$H$_9$S]. The mixture was dissolved in 30 mL of acetonitrile. The resulting yellow solution was stirred for 30 min and then it was filtered through Celite to remove NaCl. The solvent was vacuum removed leaving an orange-yellow residue, which was dissolved in a minimum amount of THF. Diethyl ether and hexane were added to precipitate a yellow-orange solid. The supernatant liquid was removed by cannula. The solids were washed three times with hexane and dried under vacuum (1.02 g, 63% yield). Anal. Calcd (Found) (Galbraith Laboratories, Knoxville, TN) for [PPN][1(*t*-Bu)], C$_{45}$H$_{39}$O$_5$P$_2$NSCr: C, 65.93 (66.35); H, 4.79 (4.83); S, 3.91 (3.57). IR (ν(CO), THF): [PPN][1(*t*-Bu)] 2034 w, 1918 s, 1894 s, 1850 m; [PPN][1(Et)] 2034 w, 1905 s, 1850 m cm^{-1}. ^{1}H NMR (acetone-d_6): [PPN][1(*t*-Bu)] 1.35 (CH$_3$, s) ppm; [PPN][1(Et)] 2.29 (CH$_2$, q), 1.18 (CH$_3$, t), ppm; ^{13}C NMR (acetone-d_6): [PPN][1(*t*-Bu)] 228.6 (1 CO), 223.6 (4 CO) ppm; [PPN][1(Et)] 227.5 (1 CO), 222.4 (4 CO) ppm.

B. [PPN][RS[Cr(CO)$_5$]$_2$] ([PPN][2(R)]); R = *t*-C$_4$H$_9$, C$_2$H$_5$, *i*-C$_3$H$_7$, CH$_3$, H. In a typical preparation, 1.28 g (1.56 mmol) of [PPN][1(*t*-Bu)] was placed in a 100-mL Schlenk flask to which 60 mL of THF·Cr(CO)$_5$, freshly prepared by photolysis of 0.370 g (1.68 mmol) of Cr(CO)$_6$ in THF, was added. The mixture was stirred for 10 min, followed by vacuum removal of the solvent. The residue was dissolved in 5 mL of diethyl ether, and pentane was added to precipitate out an orange solid. The solid was washed with pentane and vacuum dried to yield 0.820 g of [PPN][2(*t*-Bu)] (52% yield). Representative IR (ν(CO), THF): [PPN][2(*t*-Bu)] 2053 w, 2037 w, 1960 m (sh), 1935 s, 1926 s, 1894 m, 1869 s; [PPN][2(*i*-Pr)] 2058 w, 2042 w, 1968 m, 1939 s, 1930 s, 1902 m, 1872 m; [PPN][2(Et)] 2053 w, 2036 w, 1961 m (sh), 1929 vs, 1900 m, 1869 m cm^{-1}.

C. [Et$_4$N][PhS[Cr(CO)$_5$]$_2$] ([Et$_4$N][2(Ph)]). Freshly prepared Cr(CO)$_5$·THF (40 mL, 4.5 mmol) was transferred by cannula into a flask containing [Et$_4$N][SPh] (0.54 g, 2.3 mmol). The mixture was stirred for 20 min until the IR spectrum showed the reaction to be complete. The solvent was removed by vacuum, and the crude solid was recrystallized from diethyl ether/pentane to give 0.97 g of a yellow-orange solid (69% yield). IR (ν(CO), THF): 2061 w, 2046 w, 1977 s, 1938 s, 1919 m, 1872 m cm^{-1}.

3. Oxidation of RSCr(CO)$_5^-$ with [η^5-C$_5$H$_5$)$_2$Fe][BF$_4$] ([Fc][BF$_4$]). A. (*t*-C$_4$H$_9$)SCr(CO)$_5^-$. [PPN][1(*t*-Bu)] (0.05 g, 0.061 mmol) was added to a Schlenk tube, dissolved in 5 mL of THF, and cooled to −78 °C. Five milliliters of a CH_2Cl_2 solution of [Fc][BF$_4$] (0.017 g, 0.062 mmol) was added dropwise with stirring. The blue [Fc][BF$_4$] solution was instantly quenched as it was added to the yellow-orange THF solution of [PPN][1(*t*-Bu)]. The IR (ν(CO)) spectrum of this solution, taken immediately, showed bands at 2070 w, 1939 s, and 1897 m cm^{-1}. The solvent was removed by vacuum, and the residue was extracted with hexane. IR analysis of the hexane solution showed bands at 2071 w, 1953 s, 1940 s, 1930 m, and 1914 w cm^{-1}.

B. (C$_2$H$_5$)SCr(CO)$_5^-$. The THF solution of 1(Et)$^-$/Fc$^+$, obtained as described above, had ν(CO) bands at 2072 (w), 2027 (w), 1943 (s), and 1895 (m) cm^{-1}. Upon vacuum removal of solvent, the residue was extracted with hexane to give a clear golden orange solution. An IR spectrum of this solution showed bands at 2072 (w), 2028 (w), 2006 (w), 1972 (m), 1949 (s), 1937 (m), and 1915 (w) cm^{-1}.

4. Attempted Preparation of Cr(CO)$_5$(μ-(*t*-Bu)SS(*t*-Bu))Cr(CO)$_5$ (3(*t*-Bu)). Reaction of 2 equiv of Cr(CO)$_5$·THF with 1 equiv of *tert*-butyl disulfide in THF resulted, after 2 h, in a yellow solution. The solvent was removed in vacuo, and the oil residue was taken up in hexane. The IR spectrum revealed bands at 2070 (w), 1988 (s), 1952 (s), 1941 (s), 1930 (m) (sh), and 1914 (w) cm^{-1}. The 1988-cm^{-1} band belongs to unreacted Cr(CO)$_5$·THF.

5. EPR Study: Low-Temperature Oxidations of RS[Cr(CO)$_5$]$_2^-$ and RSCr(CO)$_5^-$. All low-temperature oxidations were performed in a N_2 glovebox using a cold well to maintain the solutions at or below −70 °C. Typically, 1 mL of a 0.01 M THF or 2-MeTHF solution of [PPN][1(R)] or [PPN][2(R)] was prepared in a small vial and cooled to −78 °C. One equivalent (200 μL) of a cold 0.05 M CH_2Cl_2 solution of [Fc][BF$_4$] was added with stirring. With 1(R)$^-$, the blue color of [Fc][BF$_4$] was instantly quenched resulting in yellow solutions. With 2(R)$^-$, deep-magenta solutions were obtained instantly. By use of a chilled syringe an appropriate amount of the solution was quickly transferred to a 4 × 2.3 mm EPR tube, which was also maintained at or below −70 °C in a cylindrical brass block. The brass block and tube were removed from the glovebox, and the EPR tube was immediately immersed in liquid nitrogen for transfer to the EPR cavity kept at −80 °C.

Analogous low-temperature oxidations were carried out on ^{13}CO-enriched 2(R)$^-$. The ^{13}CO enrichment was carried out as follows. In the glovebox, 1 mL of a 0.01 M THF solution of [PPN][2(R)] in a 5-mm quartz tube was saturated with ^{13}CO by a fine trickle of the gas through a long, thin syringe needle reaching to the bottom of the tube. The tube was capped quickly to maintain a ^{13}CO atmosphere above the liquid and was transferred to the photoreactor described above, where it was irradiated for 1 min. The procedure was repeated a second time. After the second irradiation, an IR (ν(CO)) spectrum indicated substantial ^{13}CO enrichment of 2(R)$^-$.

6. IR Study: Low-Temperature Oxidations of RS[Cr(CO)$_5$]$_2^-$. Typically, to 3 mL of a 0.01 M CH_2Cl_2 solution of [PPN][2(R)] in a small vial at −70 °C was added 1 equiv of [Fc][BF$_4$] (600 μL of a 0.05 M CH_2Cl_2 solution), using a chilled syringe. The cell was filled and transferred to the IR spectrometer, using the precautions described above to avoid warming of the reaction mixture prior to spectral examination.

7. Electrochemical Studies. Cyclic voltammograms were carried out in a nitrogen glovebox, using a home-built potentiostat allowing IR compensation through positive feedback at faster potential scan rates.[16] A digital oscilloscope (Nicolet 3091) was used to acquire and measure the transient voltammograms. Potentials were measured with reference to a Ag/AgBF$_4$ (0.02 M) electrode in THF containing [*n*-Bu$_4$N][BF$_4$] (0.3 M). Each of the data points in Figure 3 was measured three times, and the resulting error was estimated to be ±2 mV. The same error was obtained for ferrocene under the same conditions. The working electrodes were the circular cross sections of gold wires of either 0.125-mm diameter (for fast voltage scan rates) or 0.50-mm diameter (for slower scan rates) sealed in Pyrex. The counter electrode was a platinum wire spiral of approximately 1-cm^2 effective area. The cell required 10 mL of test solution and 2 mL of supporting electrolyte solution for the side-arm compartment segregating the reference electrode from the test solution by means of two fine frits. [*n*-Bu$_4$N][BF$_4$] (0.3 M) was used as supporting electrolyte in THF, and the concentration of the active substrate was generally 0.002 M.

8. Molecular Orbital Calculations. MO calculations were performed using the Du Pont implementation of the extended Hückel method.[17] These calculations included the use of the two-body repulsions introduced by Anderson.[18] The parameters were obtained from the literature.[17]

9. X-ray Structural Analyses. A summary of the crystallographic results is presented in Table IV. All data sets were collected at low temperatures on Enraf-Nonius CAD4 diffractometers with graphite-filtered Mo radiation. The solution and refinement of the structures were performed on a VAX cluster system with a local program set. The heavy-atom positions were obtained via automated Patterson analysis and used to phase the reflections for the remaining light atoms via the usual combination of structure factor, Fourier synthesis, and full-matrix least-squares refinement. All non-hydrogen atoms were refined anisotropically, and the hydrogen atoms were placed in idealized positions with fixed (0.95 Å) bond lengths. Selected bond distances and angles for the anions 1(*t*-Bu)$^-$ and 2(*t*-Bu)$^-$ are given in Tables V and VI. Full tables of positional and thermal parameters, including those of the countercations, of calculated hydrogen atom positions, and of structure factor listings are available as supplementary material.

Results and Discussion

Synthesis. A variety of preparative methods have been reported for the synthesis of group VI mononuclear and binuclear thiolates.[19] In our hands, the most efficient for RSCr(CO)$_5^-$ has been

(16) Howell, J. O.; Kuhr, W. G.; Ensman, R. E.; Wightman, R. M. *J. Electroanal. Chem.* **1986**, *209*, 77.

(17) (a) Pensak, D. A.; McKinney, R. J. *Inorg. Chem.* **1979**, *18*, 3407. (b) Pensak, D. A.; McKinney, R. J. *Inorg. Chem.* **1979**, *18*, 3413.

(18) (a) Anderson, A. B. *J. Chem. Phys.* **1975**, *62*, 1187. (b) Anderson, A. B. *J. Am. Chem. Soc.* **1978**, *100*, 1153.

(19) (a) Schlientz, W. J.; Ruff, J. K. *Inorg. Chem.* **1972**, *11*, 2265. (b) Beck, W.; Tadros, S. Z. *Anorg. Allg. Chem.* **1970**, *375*, 231. (c) Cooper, M. K.; Saporta, J.; McPartlin, J. *J. Organomet. Chem.* **1977**, *133*, C33. (d) Gingerich, R. G. W.; Angelici, R. J. *J. Am. Chem. Soc.* **1979**, *101*, 5604. (e) Cooper, M. K.; Duckworth, P. A.; Henrick, K.; McPartlin, M. *J. Chem. Soc., Dalton Trans.* **1981**, 2357. (f) Darensbourg, D. J.; Rokicki, A.; Kudaroski, R. *Organometallics* **1982**, *1*, 1161. (g) Cooper, M. K.; Duckworth, P. A.; Saporta, M.; McPartlin, M. *J. Chem. Soc., Dalton Trans.* **1980**, 570. (h) Hausmann, H.; Höfler, M.; Kruck, T.; Zimmermann, H. W. *Chem. Ber.* **1981**, *114*, 975.

the reaction of $ClCr(CO)_5^-$ with sodium mercaptides (eq 1).

$$ClCr(CO)_5^- + Na^+SR^- \xrightarrow{CH_3CN} \underset{\mathbf{1}(R)^-}{RSCr(CO)_5^-} + NaCl \quad (1)$$

The binuclear chromium thiolates are readily prepared by the reaction of the mononuclear thiolates with photochemically generated $Cr(CO)_5$·THF (eq 2).

$$RSCr(CO)_5^- + Cr(CO)_5{\cdot}THF \xrightarrow{THF} \underset{\mathbf{2}(R)^-}{RS[Cr(CO)_5]_2^-} \quad (2)$$

Three-band patterns were observed for $\mathbf{1}(R)^-$ in the ν(CO) region of the IR as expected for complexes of near-C_{4v} symmetry. For $\mathbf{1}(t\text{-Bu})^-$, however, the strong E band is split, resulting in four observed bands. This splitting is presumably the result of the slight deviation from octahedral geometry caused by the bulky *tert*-butyl group (cf. X-ray structure of Figure 5). The binuclear thiolate complexes $\mathbf{2}(R)^-$, on the other hand, exhibit a complex pattern in the ν(CO) region, consistent with their low symmetry (cf. X-ray structure of Figure 6).

Chromium Thiolate Oxidations and Infrared Spectra of Oxidation Products. The blue color of $[Fc][BF_4]$ in CH_2Cl_2 was instantly discharged on addition of this reagent to equimolar solutions of yellow $\mathbf{1}(R)^-$ in THF or CH_2Cl_2 at −78 °C. Attempts to isolate a major product produced only oils (R = *t*-Bu, *i*-Pr, and Et). Significantly, however, the ν(CO) of the IR spectra of these products in hexane were indistinguishable from those obtained in attempted preparations of the sulfur–sulfur coupled dimers $Cr(CO)_5(\mu\text{-RSSR})Cr(CO)_5$ by reaction of the organic disulfide with $Cr(CO)_5$·THF (cf. Experimental Section). These observations seemed to strongly favor path A in Scheme I until this path was shown to be totally irreconciliable with the electrochemical results. The latter leave no doubt that the intermediate $RSCr(CO)_5^{\bullet}$ radicals undergo unimolecular fragmentation extremely rapidly (vide infra). A literature search provided a satisfactory explanation by revealing several examples of monodentate disulfide $M(CO)_5$ (M = Cr, Mo, W) complexes,[20] including $[CH_3SSCH_3]Cr(CO)_5$ isolated as an oil,[21] with ν(CO) regions of the IR spectra exceedingly similar to those obtained in this work either by ferrocenium oxidation of $\mathbf{1}(R)^-$ or by reaction of the organic disulfide with $Cr(CO)_5$·THF. These oxidations would appear, therefore, to follow path C of Scheme I, and the resulting organic disulfides react with only one $Cr(CO)_5$ fragment to yield the observed monodentate disulfide complexes $\mathbf{5}(R)$ (eq 3).

$$Cr(CO)_5 + RSSR \rightarrow \underset{\mathbf{5}(R)}{[RSSR]Cr(CO)_5} \quad (3)$$

Oxidation of the binuclear RS-bridged thiolates $\mathbf{2}(R)^-$ with $[Fc][BF_4]$ also occurs instantaneously at −78 °C, resulting in the formation of deep-magenta solutions that are generally stable below −25 °C. On being warmed to room temperature, the solutions become light yellow, and IR analyses show again the formation of the monodentate disulfide complexes $\mathbf{5}(R)$ together with some $Cr(CO)_6$. The latter are evidently the decomposition products of the initially formed deeply colored $RS[Cr(CO)_5]_2^{\bullet}$ radical species, which fragment into short-lived $\mathbf{1}(R)^{\bullet}$ radicals and $Cr(CO)_5$ fragments (eq 4), which in turn undergo the reactions described above (Scheme I, path C and eq 3).

$$\underset{\mathbf{2}(R)^-}{RS[Cr(CO)_5]_2^-} \xrightarrow{-e} \underset{\mathbf{2}(R)^{\bullet}}{RS[Cr(CO)_5]_2^{\bullet}} \rightarrow \underset{\mathbf{1}(R)^{\bullet}}{RSCr(CO)_5^{\bullet}} + Cr(CO)_5 \quad (4)$$

The IR (ν(CO)) spectra of the thermally labile $RS[Cr(CO)_5]_2^{\bullet}$ radicals could be obtained by means of a simple low-temperature IR cell as described in the Experimental Section. Figure 1 compares the IR spectra of the $\mathbf{2}(t\text{-Bu})^{\bullet}$ radical and of its diamagnetic anionic precursor $\mathbf{2}(t\text{-Bu})^-$, and Table I lists the IR CO stretching frequencies for a series of $\mathbf{2}(R)^{\bullet}$ radicals. No bands for bridging CO ligands were found. The observation of six bands for both the anions and the neutral radicals is consistent with very low symmetry for both species (nine bands predicted for C_s symmetry) and with some structural change in going from the anion to the radical since the band patterns are not identical. The most likely structural change for the radical is an increased planarity at the trigonal sulfur (vide infra and Figure 6). As expected for one-electron oxidation without marked structural change, the band positions in the neutral radicals have been shifted approximately 55 cm^{-1} higher in energy compared to the anions.

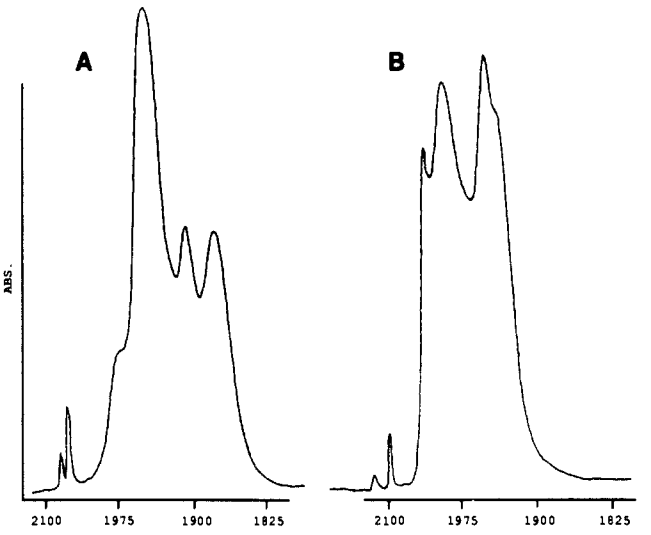

Figure 1. Infrared spectra in the CO stretching region of [PPN][*t*-BuS[Cr(CO)$_5$]$_2$](THF) and *t*-BuS[Cr(CO)$_5$]$_2^{\bullet}$ (CH_2Cl_2, −60 °C). The absorbance scale is not the same for the two spectra.

Table I. Infrared CO Stretching Frequencies for $RS[Cr(CO)_5]_2^{\bullet}$ in CH_2Cl_2

R	temp, °C	ν(CO), cm^{-1}
t-C_4H_9	−60	2122 w, 2089 w, 2007 m, 1984 s, 1940 s, 1932 s (sh)
C_2H_5	−45	2122 w, 1092 w, 2013 m, 1981 s, 1945 s (sh), 1935 s
i-C_3H_7	−65	2121 w, 2090 w, 2011 m, 1983 s, 1943 s, 1933 s (sh)
CH_3	−32	2125 w, 2092 w, 2014 m, 1983 s, 1948 s (sh), 1935 s

Table II. Cyclic Voltammetric Data for $RSCr(CO)_5^-$ and $RS[Cr(CO)_5]^{2-}$ [a]

complex[b]	E_p, V	$E_1°$, V	$E_2°$, V	ΔE_{p1},[c] V	ΔE_{p2},[c] V
$EtSCr(CO)_5^-$	−0.79				
i-$PrSCr(CO)_5^-$	−0.78				
t-$BuSCr(CO)_5^-$	−0.74				
$EtS[Cr(CO)_5]_2^-$		−0.36	0.08	0.088	0.099
i-$PrS[Cr(CO)_5]_2^-$		−0.36	0.14	0.086	0.101
t-$BuS[Cr(CO)_5]_2^-$		−0.28	0.23	0.090	0.123

[a] In THF with 0.3 M $(n\text{-Bu})_4N^+BF_4^-$. E_p and $E°$ are given vs Ag/$AgBF_4$ (0.02 M) in THF and were measured at potential scan rates of 100 mV/s. In this medium and with this reference electrode, $E°$ for ferrocene/ferrocenium (1+) is 0.226 V. [b] PPN^+ countercation. [c] $\Delta E_{pn} = E_p(ox) - E_p(red)$ at 100 mV/s; for ferrocene, $\Delta E_p = 0.075$ V in this medium at the same voltage scan rate.

Electrochemical Studies. Cyclic voltammetry shows that the mononuclear chromium thiolate anions $\mathbf{1}(R)^-$ (R = Et, *i*-Pr, *t*-Bu), easily undergo chemically irreversible oxidations in THF at room temperature at potentials that depend only very weakly on the nature of the alkyl group R (Table II, Figure 2A, wave O_1). No indication of chemical reversibility was obtained even at voltage sweep rates as high as 500 V/s. Since the oxidations are monoelectronic (vide infra), this limits the lifetime of the neutral radical $RSCr(CO)_5^{\bullet}$ to less than 50 μs.

To establish whether the intermediate radical disappears by rapid dimerization or by unimolecular fragmentation, or put

(20) (a) Abel, E. W.; Bhargava, S. K.; Mittal, P. K.; Orrell, K. G.; Sik, V. *J. Chem. Soc., Dalton Trans.* **1985**, 1561. (b) Abel, E. W.; Moss, I.; Orrell, K. G.; Aqreshi, K. B.; Sik, V.; Stephenson, D. *J. Chem. Soc., Dalton Trans.* **1988**, 1489.

(21) Ehrl, W.; Vahrenkamp, H. *Chem. Ber.* **1970**, *103*, 3563.

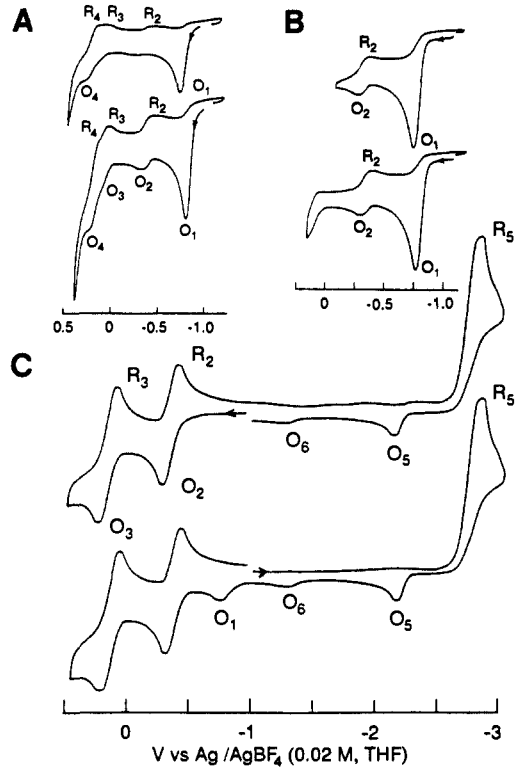

Figure 2. Cyclic voltammograms (THF, 0.3 M [n-Bu_4N][BF_4]) of (A) $EtSCr(CO)_5^-$ at 1 V/s (upper CV) and 100 mV/s (lower CV), (B) $EtSCr(CO)_5^-$ at 100 mV/s for two different anodic turning potentials, and (C) i-$PrS[Cr(CO)_5]_2^-$ at 100 mV/s initiated in the anodic (upper CV) and cathodic sense (bottom CV).

another way, whether the irreversible reaction following one-electron oxidation is kinetically second order or first order, the dependence of the peak oxidation potential on the potential scan rate was examined for the derivatives of **1** with R = Et and i-Pr. For a following reaction of first order, $\partial E_p/\partial(\log v)$ is approximately $30/n$ mV/log v, where n is the number of electrons exchanged in the electrode process, whereas for a second-order following reaction, with $n = 1$, E_p shifts only 20 mV for a 10-fold change in voltage scan rate.[22,23] Figure 3 shows the E_p vs log v dependence for R = Et together with two straight lines passing through E_p at the lowest voltage scan rate (50 mV/s) with slopes of 30 and 20 mV/log v, respectively. The line with the 30 mV/log v slope clearly agrees quite satisfactorily with the experimental behavior at lower scan rates. The two slopes can be clearly distinguished from each other even if Figure 3 included error bars corresponding to the estimated ±2 mV error in the measurement of E_p (cf. Experimental Section). At higher voltage sweep rates, a slight curvature is observed in the experimental points owing to a partial kinetic control by the rate of electron transfer at the electrode. The same effect could also arise from ohmic drop factors. This is quite unlikely for the potential sweep rates of Figure 3, however, since the IR drop was carefully electronically compensated (cf. Experimental Section). Entirely analogous results were obtained for $\mathbf{1}(i\text{-Pr})^-$.

The same measurements were also carried out for five different substrate concentrations from 0.5×10^{-3} to 5×10^{-3} M. No shift in E_p was observed with these changes in concentration, and exactly the same slope was obtained for the E_p vs log v dependence at all concentrations. We can conclude, therefore, that the chemically irreversible oxidation of $\mathbf{1}(R)^-$ is clearly monoelectronic ($n = 1$), that the following reaction is first order with respect to the intermediate radical $\mathbf{1}(R)^\bullet$, and that there is no reaction of the latter with the starting substrate $\mathbf{1}(R)^-$. Such a reaction would introduce a variation of E_p with the concentration of $\mathbf{1}(R)^-$ of 30 mV for a 10-fold increase in concentration.[22] The intermediate radical $\mathbf{1}(R)^\bullet$ clearly undergoes first-order reaction. The most plausible first-order reaction is the homolysis of the sulfur–chromium bond to yield a 16-electron $Cr(CO)_5$ fragment and an alkylthiyl radical RS$^\bullet$. The latter rapidly dimerizes to the disulfide RSSR presumably with diffusion-controlled kinetics[12,24] (Scheme I).

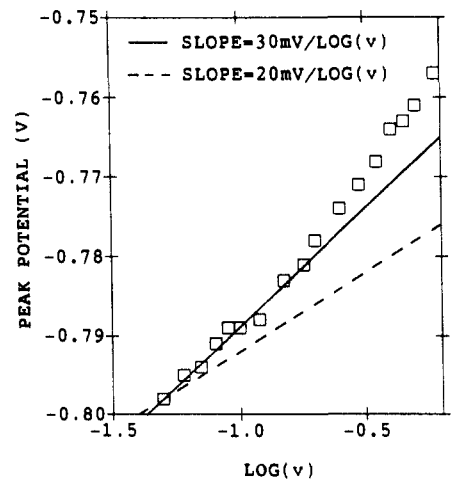

Figure 3. Dependence of the peak oxidation potential for $EtSCr(CO)_5^-$ (wave O_1, Figure 2A, same conditions) on the logarithm of the voltage scan rate.

Additional effects confirm this mode of fragmentation and add further insight concerning the chemical behavior following initial oxidation. The cyclic voltammogram of Figure 2A for $EtSCr(CO)_5^-$, extended in the anodic direction past the irreversible oxidation wave O_1, shows three reversible oxidation waves O_2, O_3, and O_4. Two of these, O_2 and O_3, are much more prominent at the slower (100 mV/s, lower CV) than at the faster voltage scan rate (1V/s, upper CV). It will be shown below that O_2 and O_3 correspond to the first and second reversible one-electron oxidations of the binuclear chromium thiolate anion $EtS[Cr(CO)_5]_2^-$, while O_4 is provisionally assigned to the oxidation of the main product of electrolysis, the monodentate disulfide complex $[EtSSEt]Cr(CO)_5$ which is also obtained when $\mathbf{1}(Et)^-$ is oxidized with ferrocenium tetrafluoroborate. At potentials more positive than O_4, the anodic current increases steeply presumably because of multielectron oxidative degradation of the chromium complexes in solution. Analogous behavior was observed for the i-Pr and t-Bu derivatives of $\mathbf{1}(R)^-$.

The formation of the binuclear thiolate $EtS[Cr(CO)_5]_2^-$ and of the monodentate disulfide complex $[EtSSEt]Cr(CO)_5$ can be explained by the reactions of the $Cr(CO)_5$ fragments, formed at O_1, with the starting complex $\mathbf{1}(Et)^-$, a process analogous to eq 2 used for the synthesis of $\mathbf{2}(R)^-$, and with the ethyl disulfide, which is also formed at O_1 by the dimerization of EtS$^\bullet$ radicals (eq 3). The dependence of the amplitudes of the O_2/R_2 and O_3/R_3 waves on the potential scan rate (cf. Figure 2A) is then qualitatively understandable by assuming relatively slow kinetics, on the time scale of cyclic voltammetry, for the reaction of $Cr(CO)_5$ fragments with the starting thiolate. At slower scans the reaction time is longer, and the accumulated product is consequently more abundant, yielding larger electrode currents. The observation of a greater amplitude for R_2 than for O_2 (Figure 2A) is also related simply to longer reaction times at R_2 than at O_2. The reaction time at R_2 can also be prolonged by extending the anodic limit of the cycle, as in Figure 2B (bottom), which shows an R_2 wave of slightly greater amplitude when the anodic excursion, and consequently the reaction time, is greater.

(22) Nadjo, L.; Savéant, J. *Electroanal. Chem.* **1973**, *48*, 113.
(23) Bard, A. J.; Faulkner, L. R. *Electrochemical Methods*; John Wiley & Sons: New York, 1980; pp 453 ff.

(24) An alternative sequence of events, indistinguishable by cyclic voltammetry from the above mechanism, would be the attack of RS$^\bullet$ on the sulfur atom of unreacted $RSCr(CO)_5^-$ to produce the radical anion $[RS(R)SCr(CO)_5]^{\bullet-}$ which, at the relatively positive potential at which it is formed, would immediately transfer an electron to the electrode to give directly the final product of oxidation, i.e., the monodentate $Cr(CO)_5$ disulfide complex **5**(R).

Table III. EPR Parameters for $RS[Cr(CO)_5]_2^{\bullet}$ in THF/CH_2Cl_2

	R					
	CH_3	C_2H_5	i-C_3H_7	t-C_4H_9	C_6H_5[a]	H
temp, °C	−70	−70	−60	−80	−50	−70
g_{iso}	2.0244	2.0245	2.0249	2.0264	2.0244	2.0264
a(H), G	6.3[e]	3.0[f]				ca. 4.0[d]
$a(^{53}Cr)$, G	5.3	5.4	6.0	5.0	5.5	
$a(^{33}S)$, G	14.9	14.6	14.5	14.2	13.4	
g_1[b]	2.0437	2.0426	2.0457	2.0496	2.0413	2.0471
g_2[b]	2.0274	2.0268	2.0282	2.0268	2.0269	2.0326
g_3[b]	2.0025	2.0035	1.9991	1.9998	2.0024	2.0018
g_{av}[c]	2.0245	2.0243	2.0243	2.0254	2.0235	2.0272

[a] In pentane. [b] In 2-MeTHF at −170 °C. [c] $g_{av} = (g_1 + g_2 + g_3)/3$. [d] Partially resolved doublet. [e] Quartet. [f] Triplet.

The binuclear thiolate complexes $2(R)^-$ can also be easily electrochemically oxidized, albeit not as readily as their mononuclear analogues (Table I). Indeed, they can be reversibly oxidized not only to the corresponding neutral radical species $2(R)^{\bullet}$, but also to the corresponding monocations $2(R)^+$ (Scheme II). The latter are organometallic sulfonium cations, isoelectronic with the well-characterized neutral binuclear phosphinidene complexes $RP[Cr(CO)_5]_2$.[13-15] No attempt was made in this study to further characterize and to isolate these novel sulfonium salts. An oxidant more potent than Fc^+, however, will be needed for their preparation from $2(R)^-$.

Two cyclic voltammograms for i-$PrS[Cr(CO)_5]_2^-$ are shown in Figure 2C. In the upper, the initially anodic scan displaying the two reversible oxidation steps O_2 and O_3 (Scheme II) was extended in the cathodic direction to include the very tall irreversible reduction wave R_5. Control experiments with [PPN][Cl] and the considerations to follow indicate that this peak, showing a clear doubling at expanded potential scans, corresponds to the chemically irreversible reductions of both the PPN^+ countercation and the starting i-$PrS[Cr(CO)_5]_2^-$ anion. The reduction of the latter can be represented by eq 5 since oxidation waves characteristic of the mononuclear thiolate $1(R)^-$ and of the $Cr(CO)_5^{2-}$ dianion are observed following reduction at R_5. The oxidation of $1(i\text{-}Pr)^-$ at O_1 can be seen when the cyclic voltammogram is initiated in the cathodic direction (Figure 1C, bottom), while the oxidation of $Cr(CO)_5^{2-}$ gives rise to the oxidation peaks O_5 and O_6 because of the processes of eqs 6 and 7, respectively, which will be discussed in detail elsewhere.[25]

$$\underset{2(R)^-}{RS[Cr(CO)_5]_2^-} \xrightarrow{+2e} \underset{1(R)^-}{RSCr(CO)_5^-} + Cr(CO)_5^{2-} \quad (5)$$

$$Cr(CO)_5^{2-} \xrightarrow{-e} Cr(CO)_5^{\bullet -} \quad (6)$$

$$2Cr(CO)_5^{\bullet -} \rightarrow Cr_2(CO)_{10}^{2-}$$

$$Cr_2(CO)_{10}^{2-} \underset{+e}{\overset{-e}{\rightleftharpoons}} Cr_2(CO)_{10}^{\bullet -} \quad (7)$$

EPR Characterization of Radical Intermediates. The solutions obtained from the oxidation of $RSCr(CO)_5^-$ (R = Et, i-Pr, t-Bu) with 1 equiv of $[Fc][BF_4]$ at −80 °C in CH_2Cl_2 were examined by EPR without any warming (cf. Experimental Section). Only weak signals were observed, which decayed upon warming of the solutions. If 2 equiv of $[Fc][BF_4]$ were used, relatively weak spectra of the binuclear $2(R)^{\bullet}$ radicals were often observed as secondary products of oxidation. As was seen above, $2(R)^-$ can be produced in the oxidation of $1(R)^-$ by reaction of the latter with $Cr(CO)_5$ fragments. As expected from the electrochemical results, the $RSCr(CO)_5^{\bullet}$ radicals were not sufficiently long-lived to be detected by EPR in such experiments.

Intense UV photolysis of dilute pentane solutions of $Cr(CO)_6$ (0.01 M) and various disulfides RSSR (R = Me, Et, i-Pr, t-Bu; up to 10 equiv) in the ESR cavity at low temperatures also failed to give spectra attributable to $1(R)^{\bullet}$. The latter could arise by reaction of photochemically generated $RS^{\bullet}$ radicals with $Cr(CO)_5$ fragments. Relatively weak spectra of several thermally labile unknown species were obtained instead. The strongest signals, however, were unmistakably due to $2(R)^{\bullet}$ radicals. Particularly intense spectra of these radicals were obtained when the irradiation was carried out in a low-temperature photoreactor (cf. Experimental Section) followed by transfer of the samples to the EPR cavity in liquid nitrogen to avoid warming before spectral examination.

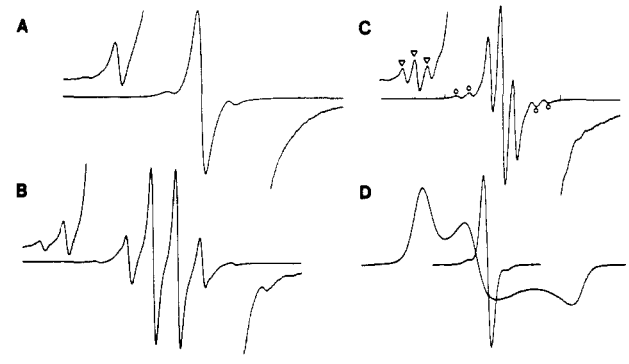

Figure 4. EPR spectra in THF/CH_2Cl_2 at −80 °C of (A) t-$BuS[Cr(CO)_5]_2^{\bullet}$, (B) $MeS[Cr(CO)_5]_2^{\bullet}$, (C) $EtS[Cr(CO)_5]_2^{\bullet}$, and (D) i-$PrS[Cr(CO)_5]_2$. (Superposed powder spectrum, appropriate for three different principal g-tensor components, was obtained at −170 °C.) Sections A–C also have parts of the spectra at high amplification (×100) to show the ^{33}S satellite lines [e.g., triangles in section C, which also shows (circles) ^{53}Cr satellite lines]. The horizontal scale is 70 G for each full spectral scan.

The relative stability of the $2(R)^{\bullet}$ radical species produced electrochemically upon one-electron oxidation of the binuclear thiolates $2(R)^-$ was confirmed by EPR spectroscopy. The oxidations of $2(R)^-$ (R = H, Me, Et, t-Bu, i-Pr, Ph) in CH_2Cl_2 or THF at −80 °C with 1 equiv of $[Fc][BF_4]$ in CH_2Cl_2 resulted in deep-magenta solutions exhibiting very strong EPR spectra of $2(R)^{\bullet}$, which decayed slowly at temperatures above −30 °C. The phenyl derivative was more stable, decomposing slowly above 0 °C.

The solution EPR spectra of $2(R)^{\bullet}$ with R = Me, Et, i-Pr, and t-Bu are shown in Figure 4 together with a typical powder spectrum of a frozen solution (R = i-Pr, Figure 4D). The latter reveals three distinct principal components of the g tensor, which average correctly to the isotropic g values of the solution spectra (Table III). Proton hyperfine coupling was detected for R = H, Me, and Et, resulting in a splitting of the EPR absorption into a doublet, quartet, and triplet, respectively, but not for R = i-Pr, t-Bu, and Ph (Figure 4, Table III). The line widths are temperature-dependent and narrowest between −50 and −80 °C. Optimum line widths vary from 1.5 G (R = Me, Et) to ca. 4 G for $2(H)^{\bullet}$ at −90 °C in CH_2Cl_2. The spectrum of the latter radical [from either the PPN^+ or the Et_4N^+ salt of $2(H)^-$] was always contaminated by a much broader line of unknown origin with g_{iso} = 2.0365. This species has a greater g-tensor anisotropy (g_1 = 2.0769, g_2 = 2.0369, g_3 = 1.9974) and decayed more rapidly than $2(H)^{\bullet}$ on warming. The THF/CH_2Cl_2 reaction mixture obtained with $2(Ph)^-$ upon oxidation with $[Fc][BF_4]$ was diluted more than 10-fold with pentane, and strong spectra of $2(Ph)^{\bullet}$ could still be

(25) Verpeaux, J.-N.; Amatore, C.; Krusic, P. J. To be published.

Table IV. Summary of X-ray Diffraction Data for [PPN][*t*-BuSCr(CO)$_5$]·THF (A) and [PPN][*t*-BuS[Cr(CO)$_5$]$_2$] (B)

parameter	A	B
formula	$CrSP_2O_6NC_{49}H_{47}$	$Cr_2SP_2O_{10}NC_{50}H_{39}$
MW	891.93	1011.87
space group	$P2_1/c$	$C2/c$
a, Å	17.953 (4)	31.880 (7)
b, Å	17.266 (3)	13.310 (2)
c, Å	14.733 (4)	23.801 (5)
β, deg	93.89 (1)	100.74 (1)
cell vol, Å^3	4556.4	9922.3
Z	4	8
crystal dimens, mm	0.40 × 0.40 × 0.41	0.40 × 0.32 × 0.50
ρ(calc), g/cm^3	1.30	1.36
μ, cm^{-1}	4.04	5.85
temp, °C	−70	−70
radiatn, Å	Mo Kα	Mo Kα
2θ limits, deg	$2.3 \le 2\theta \le 52.0$	$1.7 \le 2\theta \le 52.0$
reflections	9511 total (4918)	10428 total (4975)
no. of parameters refined	541	595
error of fit	1.75	1.40
R^a	0.050	0.046
$R_w{}^b$	0.050	0.044

$^a \Sigma||F_o| - |F_c||/\Sigma|F_o|$. $^b [\Sigma w(|F_o| - |F_c|)^2/\Sigma wF_o^2]^{1/2}$.

Table V. Selected Bond Distances and Bond Angles for *t*-BuSCr(CO)$_5^-$

	Bond Distances, Å		
Cr–S	2.479 (1)	O2–C2	1.142 (5)
Cr–C1	1.824 (4)	O3–C3	1.158 (5)
Cr–C2	1.898 (5)	O4–C4	1.147 (5)
Cr–C3	1.868 (5)	O5–C5	1.150 (5)
Cr–C4	1.878 (5)	C6–C7	1.502 (6)
Cr–C5	1.881 (6)	C6–C8	1.496 (7)
S–C6	1.837 (5)	C6–C9	1.516 (6)
O1–C1	1.163 (5)		
	Bond Angles (deg)		
S–Cr–C1	170.9 (2)	C3–Cr–C4	172.9 (2)
S–Cr–C2	85.1 (1)	C3–Cr–C5	93.3 (2)
S–Cr–C3	83.6 (1)	C4–Cr–C5	91.0 (2)
S–Cr–C4	102.7 (1)	Cr–S–C6	114.5 (1)
S–Cr–C5	82.0 (1)	Cr–C1–O1	179.1 (5)
C1–Cr–C2	96.6 (2)	Cr–C2–O2	176.8 (4)
C1–Cr–C3	87.6 (2)	Cr–C3–O3	175.3 (4)
C1–Cr–C4	86.2 (2)	Cr–C4–O4	172.9 (4)
C1–Cr–C5	96.4 (2)	Cr–C5–O5	176.9 (5)
C2–Cr–C3	86.5 (2)	S–C6–C7	111.7 (3)
C2–Cr–C4	90.6 (2)	S–C6–C8	111.0 (3)
C2–Cr–C5	167.0 (2)	S–C6–C9	106.0 (3)

obtained, consistent with a neutral hydrocarbon-soluble radical species.

The solution spectra of all **2**(R)$^\bullet$ radicals, except that of **2**(H)$^\bullet$ with a much broader line width, displayed easily observable satellite lines due to ^{53}Cr ($I = {}^3/_2$, 9.55% natural abundance, e.g., lines marked with circles in Figure 4C). Generally, these were only the outermost lines of the ^{53}Cr 1:1:1:1 quartets. From the positions of these outermost lines, the ^{53}Cr isotropic hyperfine splitting could nevertheless be extracted easily [$a(^{53}Cr)$ is $^2/_3$ the separation between the outermost satellite line and the corresponding line of the main spectrum]. This splitting is rather insensitive to the nature of R and averages ca. 5.5 G.

Amplification of the spectra (×100) revealed additional weak satellite lines, which could arise from coupling with a ^{13}C ($I = {}^1/_2$, 1.108%) or a ^{33}S ($I = {}^3/_2$, 0.76%) nucleus (e.g., Figure 4C, triangles). The upfield satellite lines were more difficult to detect since they are broader than those at lower magnetic fields. Assignment to ^{13}C would result in a ^{13}C isotropic hyperfine splitting of about 43 G, which is unusually large for a transition-metal carbonyl radical. It would indicate a rather large spin density on a carbon, as might be appropriate in some cases for a bridging carbonyl group.[26,27] However, ^{13}C enrichment had no effect on the relative intensities of these satellite lines: it only caused a broadening of the spectrum as expected if the hyperfine splittings of the interacting ^{13}C atoms were comparable to the line widths of the unlabeled species. These satellite lines must then be assigned to a ^{33}S coupling. In that case, the visible satellite lines are the outermost lines of 1:1:1:1 ^{33}S quartets ($I = {}^3/_2$), and the ^{33}S splitting can be extracted in exactly the same manner as for the ^{53}Cr hyperfine splitting. The ^{33}S splitting is fairly constant at about 14.5 G for all R groups (Table III) and decreases slightly for the derivative with a phenyl substituent on sulfur (13.4 G). The measured intensities of the satellite lines relative to the corresponding lines of the unlabeled species are also in agreement with the calculated relative intensities based on the isotopic natural abundance for ^{33}S.

Collectively, the observations of (a) relatively large ^{33}S splitting, (b) substantial hyperfine splitting to α protons with R = CH_3 and C_2H_5, (c) absence of bridging carbonyls indicated by low-temperature IR spectra, and (d) ΔE_p's close to those expected for chemically reversible redox processes (Table II) all strongly argue in favor of a structure for the **2**(R)$^\bullet$ radicals quite comparable to that of their anionic precursors, exemplified by that of **2**(*t*-Bu)$^-$ (Figure 6), with a large fraction of the unpaired electron density in a p_z orbital on the trigonal bridging sulfur. The lack of resolved proton splitting for **2**(*i*-Pr)$^\bullet$ would then imply a preferred conformation that keeps the α proton of the isopropyl group close to the nodal plane of the p_z orbital on sulfur. Similarly, the reduction of $a(^{33}S)$ and g_{iso} for **2**(Ph)$^\bullet$, and possibly the greater thermal stability of this derivative, would be the result of some π delocalization of the unpaired electron over the phenyl substituent.

Table VI. Selected Bond Distances and Bond Angles for *t*-BuS[Cr(CO)$_5$]$_2^-$

	Bond Distances, Å		
Cr1–S1	2.509 (1)	O1–C1	1.153 (5)
Cr2–S1	2.518 (1)	O2–C2	1.147 (5)
Cr1–C1	1.834 (5)	O3–C3	1.143 (5)
Cr1–C2	1.883 (5)	O4–C4	1.140 (5)
Cr1–C3	1.893 (5)	O5–C5	1.145 (5)
Cr1–C4	1.894 (5)	O6–C6	1.166 (6)
Cr1–C5	1.896 (5)	O7–C7	1.140 (5)
Cr2–C6	1.822 (6)	O8–C8	1.127 (5)
Cr2–C7	1.889 (5)	O9–C9	1.149 (5)
Cr2–C8	1.901 (5)	O10–C10	1.142 (5)
Cr2–C9	1.889 (5)	C1′–C2′	1.515 (7)
Cr2–C10	1.877 (5)	C1′–C3′	1.531 (6)
S–C1′	1.863 (5)	C1′–C4′	1.525 (7)
	Bond Angles, deg		
S–Cr1–C1	173.8 (2)	S–Cr2–C9	89.9 (1)
S–Cr1–C2	96.6 (2)	S–Cr2–C10	86.0 (2)
S–Cr1–C3	89.8 (1)	C1–Cr1–C2	88.7 (2)
S–Cr1–C4	83.7 (1)	C1–Cr1–C3	87.1 (2)
S–Cr1–C5	93.5 (1)	C1–Cr1–C4	90.7 (2)
S–Cr2–C6	175.9 (2)	C1–Cr1–C5	89.5 (2)
S–Cr2–C7	99.4 (2)	C2–Cr1–C3	94.1 (2)
S–Cr2–C8	88.8 2)	C2–Cr1–C4	179.3 (5)
C2–Cr1–C5	86.6 (2)	Cr1–S–C1′	113.8 (2)
C3–Cr1–C4	86.2 (2)	Cr2–S–C1′	112.4 (2)
C3–Cr1–C5	176.5 (2)	Cr1–C1–O1	176.8 (6)
C4–Cr1–C5	93.1 (2)	Cr1–C2–O2	175.5 (5)
C6–Cr2–C7	84.7 (2)	Cr1–C3–O3	173.3 (4)
C6–Cr2–C8	91.9 (2)	Cr1–C4–O4	176.4 (4)
C6–Cr2–C9	86.0 (2)	Cr1–C5–O5	175.9 (4)
C6–Cr2–C10	93.5 (2)	Cr2–C6–O6	178.6 (6)
C7–Cr2–C8	88.7 (2)	Cr2–C7–O7	173.6 (5)
C7–Cr2–C9	170.6 (2)	Cr2–C8–O8	177.4 (5)
C7–Cr2–C10	89.4 (2)	Cr2–C9–O9	174.1 (4)
C8–Cr2–C9	92.6 (2)	Cr2–C10–O10	179.3 (7)
C8–Cr2–C10	174.2 (2)	S–C1′–C2′	111.7 (4)
C9–Cr2–C10	90.1 (2)	S–C1′–C3′	107.1 (3)
Cr1–S–Cr2	117.11 (5)	S–C1′–C4′	109.5 (3)

(26) Krusic, P. J.; Jones, D. J.; Roe, D. C. *Organometallics* **1986**, *5*, 456.

(27) (a) Baker, R. T.; Krusic, P. J.; Calabrese, J. C.; Roe, D. C. *Organometallics* **1986**, *5*, 1506. (b) Baker, R. T.; Calabrese, J. C.; Krusic, P. J.; Therien, M. J.; Trogler, W. C. *J. Am. Chem. Soc.* **1988**, *110*, 8392.

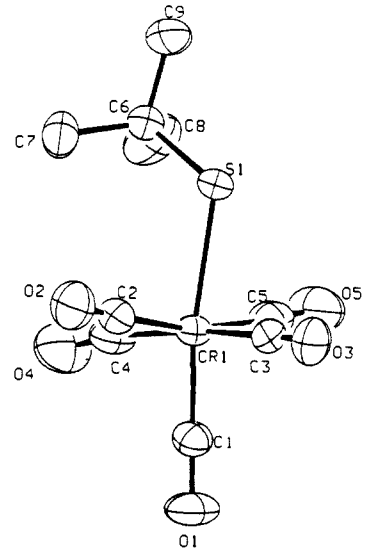

Figure 5. Molecular structure of t-BuSCr(CO)$_5^-$.

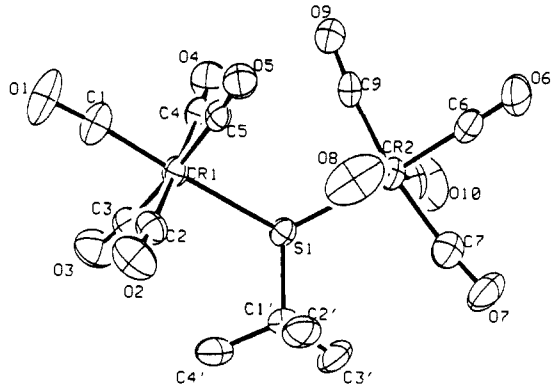

Figure 6. Molecular structure of t-BuS[Cr(CO)$_5$]$_2^-$.

These radicals can be formally considered as organometallic sulfuranyl radicals $R_3S^\bullet$, which have been studied by EPR so far only for R = F, OR, and OR_F.[12b,28] Only a few examples are known in which the sulfuranyl radical has one simple alkyl group R and two alkoxy groups attached to the trivalent sulfur. A study of the anisotropic EPR spectrum of the prototype $F_3S^\bullet$ provides strong evidence that this radical is not a π radical but rather T-shaped with the SOMO in an in-plane σ orbital.[28c] The closest organic analogue of **2**(R)$^\bullet$ appears to be $CH_3SO^\bullet$ produced by γ irradiation of dimethyl sulfoxide in a single crystal.[28g] An analysis of the anisotropic EPR spectrum of the latter was found to be consistent with the structure shown below with ca. 72% of the unpaired electron density in the sulfur 3p orbital.[28g] At very low temperatures the methyl group adopts a fixed conformation. The conformational dependence of the methyl proton coupling was exactly interpretable in terms of $a(H) = \rho_S B \cos^2 \theta$ with B = 25.4 G.[28g] Adopting this value of B for our **2**(CH$_3$)$^\bullet$ gives for the 3p spin density on sulfur ρ_S = 49.6% [a(H) = 6.3 G, $\langle\cos^2\theta\rangle = {}^1/_2$ for freely rotating CH_3] in excellent agreement with extended Hückel (EH) MO calculations (vide infra).

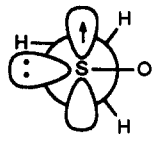

(28) (a) Morton, J. R.; Preston, K. F. *J. Phys. Chem.* **1973**, *77*, 2645. (b) Colussi, A. J.; Morton, J. R.; Preston, K. F.; Fessenden, R. W. *J. Chem. Phys.* **1974**, *61*, 1247. (c) Morton, J. R.; Preston, K. F.; Strach, S. J. *J. Chem. Phys.* **1978**, *69*, 1392. (d) Chapman, J. S.; Cooper, J. W.; Roberts, B. P. *J. Chem. Soc., Chem. Commun.* **1976**, 835. (e) Cooper, J. W.; Roberts, B. P. *J. Chem. Soc., Chem. Commun.* **1977**, 228. (f) Gara, W. B.; Roberts, B. P. *J. Organomet. Chem.* **1977**, *135*, C20. (g) Nishikida, K.; Williams, F. *J. Am. Chem. Soc.* **1974**, *96*, 4781.

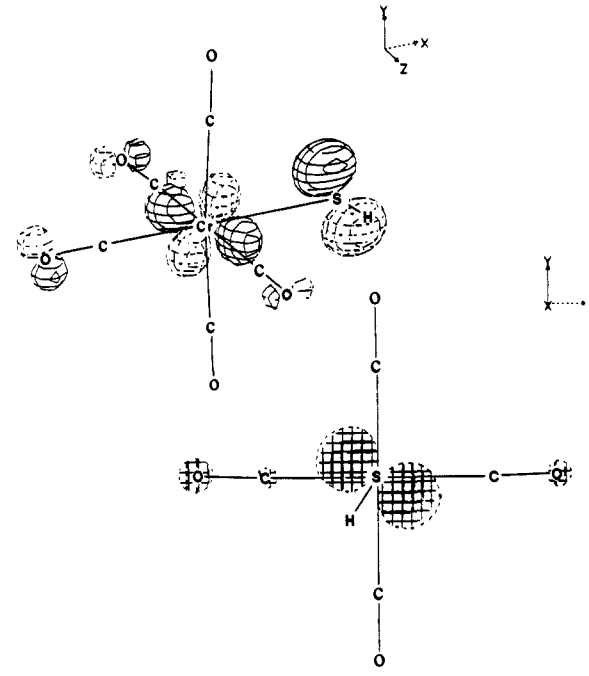

Figure 7. Two views of the SOMO of HSCr(CO)$_5^\bullet$ suggested by extended Hückel calculations.

Solid-State Structures. The X-ray structures of **1**(t-Bu)$^-$ and **2**(t-Bu)$^-$ are shown in Figures 5 and 6. In **1**(t-Bu)$^-$ the *tert*-butyl group clearly distorts the octahedral environment of the chromium atom. The Cr–S distance of 2.479 Å is exactly the same as for [Na-kryptofix-221][HSCr(CO)$_5$], which has a nearly ideal octahedral geometry at Cr.[19f] The Cr_1–S_1–C_6 bond angle is 114.5° compared with 134° for the Cr–S–H angle in the HSCr(CO)$_5^-$ anion. The average Cr–C_{eq} bond distance is 1.881 Å, and the Cr–C_{ax} distance is 1.824 Å. This shortening of the Cr–C_{ax} bond by 0.057 Å is in agreement with other sulfur and oxygen donor complexes with the formulation Cr(CO)$_5$L.[29]

The structure of **2**(t-Bu)$^-$ shows that the Cr–S–Cr bond is bent with an angle of 117.1°. The S–Cr–CO_{trans} axes are acceptably linear. The relative orientations of the pseudooctahedral Cr(CO)$_5$ units are staggered to minimize repulsions. The average Cr–S bond distance is 2.513 Å, which is approximately 0.02 Å longer than for **1**(t-Bu)$^-$. A trans influence is again observed, with the Cr–C distance trans to the sulfur approximately 0.06 Å shorter than for the other carbonyls. The bonding at the trigonal S atom is distinctly pyramidal: the S–C1′ bond forms an angle of 41.2° with the Cr_1–S–Cr_2 plane.

In general, the structure of **2**(t-Bu)$^-$ is similar to those of the related anions [PPN][$Cr_2(CO)_{10}I$][30] and [Na(18-crown-6)][$W_2(CO)_{10}(\mu$-SH)].[19e] These structures have bent M–X–M bridges of 117.9 and 124.2°, respectively. The equatorial carbonyl groups in these anions are also staggered, as observed in our study. The Cr–I bond lengths average 2.789 Å while the W–S distance is 2.591 Å. These structures, along with ours, have low symmetry, which can be best described as approaching C_s in the solid state.

Molecular Orbital Calculations. Extended Hückel molecular orbital calculations were performed for HSCr(CO)$_5^\bullet$ and HS-[Cr(CO)$_5$]$_2^\bullet$ as models for the **1**(R)$^\bullet$ and **2**(R)$^\bullet$ radicals, respectively. For HSCr(CO)$_5^\bullet$, the atomic coordinates were obtained from the X-ray structure of the anionic analogue.[19f] For HS-[Cr(CO)$_5$]$_2^\bullet$, the atomic coordinates were those of **2**(t-Bu)$^-$ in which the *tert*-butyl group was replaced by a hydrogen atom with an S–H bond distance of 1.1 Å. The shapes of the singly occupied molecular orbitals (SOMO's) for these radicals are shown in

(29) (a) Eekhof, H.; Hogeveen, H.; Kellog, R. M. *J. Organomet. Chem.* **1978**, *161*, 361. (b) Plastas, H. J.; Stewart, J. M.; Grim, S. O. *J. Am. Chem. Soc.* **1969**, *91*, 4326. (c) Baker, E. N.; Reay, B. R. *J. Chem. Soc., Dalton Trans.* **1973**, 2205.

(30) Handy, L. B.; Ruff, J. K.; Dahl, L. F. *J. Am. Chem. Soc.* **1970**, *92*, 7328.

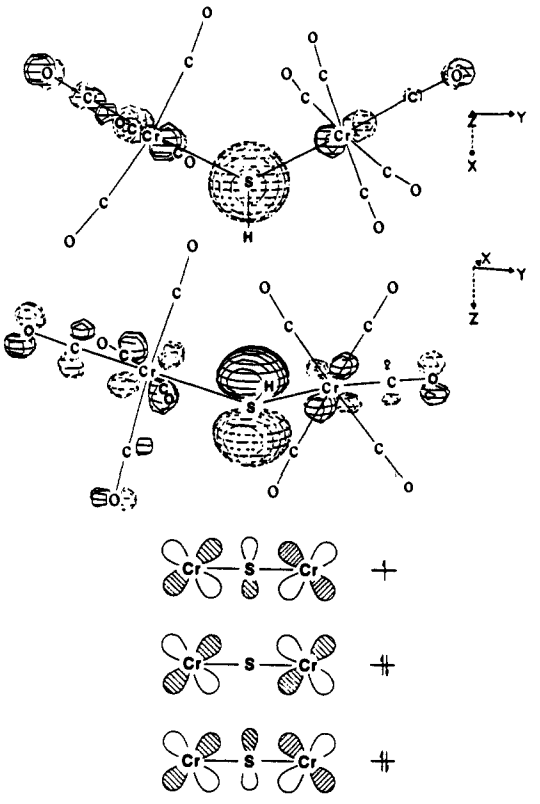

Figure 8. Two views of the SOMO of $HS[Cr(CO)_5]_2$ suggested by extended Hückel calculations and pseudoallylic bonding description for $RS[Cr(CO)_5]_2^{\bullet}$ radicals.

Figures 7 and 8 in the form of computer-generated contour lines.

It is seen that the SOMO of $HSCr(CO)_5^{\bullet}$ has a prominent component on sulfur consisting of a p-type orbital normal to the Cr–S–H plane. This orbital component would form a covalent bond by overlap with its counterpart on another $HSCr(CO)_5^{\bullet}$ radical, producing a sulfur–sulfur bond, if the S–Cr bond did not undergo facile homolysis. The unpaired electron in $HSCr(CO)_5^{\bullet}$ resides mostly in a SOMO that is antibonding between chromium and sulfur. In the chosen frame of reference and for the orientation of the SH bond found in the solid state for $\mathbf{1}(H)^-$ (Figure 7), the d_{xy} and d_{xz} orbitals are the only chromium orbitals that contribute to the SOMO. A totally analogous molecular orbital description was found[1] for $(\pi\text{-}C_5H_5)Fe(CO)_2SR$ and $(\pi\text{-}C_5H_5)Fe(CO)_2SR^{\bullet+}$, which are the electronic equivalents of $\mathbf{1}(R)^-$ and $\mathbf{1}(R)^{\bullet}$, respectively. For $\mathbf{1}(R)^-$, the orbital of Figure 7 will have, of course, double occupancy.[31]

A more quantitative picture of the unpaired electron distribution is obtained by considering the sums of the squares of the EH coefficients of the atomic orbitals that make up the SOMO. These values represent the unpaired electron populations of the contributing atomic orbitals, that is, the unpaired spin densities on atoms or groups of atoms of the radical in the EH approximation. This approximation cannot account for unpaired spin densities arising from spin-polarization effects. For $HSCr(CO)_5^{\bullet}$, we find that the unpaired spin densities are 30.1% Cr, 31.5% S, and 38.4% for the remaining atoms.

For $HS[Cr(CO)_5]_2^{\bullet}$, EH calculations predict a SOMO that is localized to a large extent on the bridging trigonal sulfur in a p-type atomic orbital π conjugated in an antibonding sense to d orbitals of the Cr neighbors (Figure 8). The unpaired spin densities are 45.7% for sulfur, an average of 9.3% for each chromium atom, an average of 8.7% for each of the two trans CO groups, which provide an extension of the π system, and 18.5% for the remaining 17 atoms. The square of the sulfur 3s EH coefficient of the SOMO gives a sulfur 3s-orbital character of 0.33%. Since a unit population of the 3s orbital on sulfur gives rise to a ^{33}S hyperfine splitting of 1237 G,[32] a 0.33% population would produce a splitting of 4.1 G, which must be compared with the observed average value of 14.5 G for a series of $\mathbf{2}(R)^{\bullet}$ radicals (Table III). The agreement is not particularly good, presumably because spin-polarization effects are neglected in the EH approximation.

EH calculations were also carried out for the binuclear phosphinidene complex $HP[Cr(CO)_5]_2$ and its radical anion as models of the corresponding alkyl phosphinidene derivatives. As was pointed out above, $RP[Cr(CO)_5]_2$ complexes are isoelectronic with the electrochemically generated $\mathbf{2}(R)^+$ sulfonium cations, while the yet undetected $RP[Cr(CO)_5]_2^{\bullet-}$ radical anions are isoelectronic with $\mathbf{2}(R)^{\bullet}$. The coordinates were those used for $HS[Cr(CO)_5]_2^{\bullet}$ except that the P–H bond was forced to be in the Cr–P–Cr plane. The resulting molecular orbitals and their energies are strikingly similar to those calculated for the sulfur analogue. They are also in accord with the idealized bonding description put forward for phosphinidene complexes[13,33] based on a pseudoallylic three-center π system schematically represented in Figure 8 for $\mathbf{2}(R)^{\bullet}$. Thus, for the phosphinidenes and $\mathbf{2}(R)^+$ there are four electrons in the π system, leaving an unoccupied orbital close in energy [0.34 eV for $\mathbf{2}(H)^+$]. The geometry at the central atom is strictly trigonal planar,[13] and electronic transitions within this π system are responsible for the strong absorptions to the visible region characteristic of phosphinidenes. For $\mathbf{2}(R)^{\bullet}$ and the hypothetical phosphinidene radical anions, the erstwhile LUMO becomes singly occupied (Figure 8). The unpaired electron, being considerably localized on sulfur, may be stereochemically active and strict planarity at sulfur need not obtain. Electronic transitions within this five-electron π system are still possible, and the radicals are deeply colored. Since the closest LUMO is much further in energy [1.79 eV for pyramidal $\mathbf{2}(H)^{\bullet}$] than the filled orbitals (a cluster of seven orbitals separated from 0.35 to 1.0 eV from the SOMO), spin–orbit interactions take place mostly with filled orbitals, and g_1 and g_2 are shifted to values that are more positive than the spin-only value (2.0023).[34] Finally, in the binuclear thiolate anions $\mathbf{2}(R)^-$, the pseudoallylic π system with six electrons is filled, the compounds no longer absorb strongly in the visible region (they are light yellow), there being no nearby empty or singly occupied orbital, and the distinct pyramidal geometry at the trigonal sulfur is the result of the presence of a stereochemically active lone pair of electrons residing principally on sulfur.

Acknowledgment. We thank Drs. David L. Thorn and Michael D. Ward for useful discussions, Steven A. Hill for technical assistance, and Edward J. Delawski for preliminary cyclic voltammetry experiments. J.S. expresses his gratitude to the Central Research and Development Department for the hospitality extended to him during part of this work. M.Y.D. acknowledges funds from the National Science Foundation (Grant CHE 86-03664) for partial support of this work. P.J.K. and C.A. are also grateful to the donors of a NATO Grant for International Collaboration in Research.

Supplementary Material Available: Complete tables of fractional coordinates, hydrogen coordinates, anisotropic thermal parameters, interatomic distances, and bond angles for $[PPN][\mathbf{1}(t\text{-Bu})]\cdot THF$ and $[PPN][\mathbf{2}(t\text{-Bu})]$ (11 pages). Ordering information is given on any current masthead page.

(31) The π antibonding between Cr and S in the SOMO of $\mathbf{1}(R)^{\bullet}$ is not the cause for the facile homolysis of the Cr–S bond, or else the parent anion $\mathbf{1}(R)^-$, with one more electron in the same orbital, would be even less stable.

(32) Morton, J. R.; Preston, K. F. *J. Magn. Reson.* **1978**, *30*, 577.

(33) Cf. also: Kostič, N. M.; Fenske, R. F. *J. Organomet. Chem.* **1982**, *233*, 337.

(34) Cf.: Goodman, B. A.; Raynor, J. B. *Adv. Inorg. Chem. Radiochem.* **1970**, *13*, 136.